Journal of Computational Physics 230 (2011) 4011–4027

Contents lists available at ScienceDirect

Journal of Computational Physics

journal homepage: www.elsevier.com/locate/jcp

Improvements on open and traction boundary conditions for Navier–Stokes time-splitting methods

A. Poux, S. Glockner *, M. Azaïez

Université de Bordeaux, UMR CNRS 5295, IPB, 16 avenue Pey-Berland, 33607 Pessac, France

ARTICLE INFO

Article history:
Received 5 November 2010
Received in revised form 4 February 2011
Accepted 16 February 2011
Available online 22 February 2011

Keywords:
Navier–Stokes equations
Projection methods
Pressure-correction methods
Fractional step methods
Traction boundary condition
Open boundary condition
Pressure boundary condition
Bifurcated tube
Square cylinder

ABSTRACT

We present in this paper a numerical scheme for incompressible Navier–Stokes equations with open and traction boundary conditions, in the framework of pressure-correction methods. A new way to enforce this type of boundary condition is proposed and provides higher pressure and velocity convergence rates in space and time than found in the present state of the art. We illustrate this result by computing some numerical and physical tests. In particular, we establish reference solutions of a laminar flow in a geometry where a bifurcation takes place and of the unsteady flow around a square cylinder.

1. Introduction

The main difficulty in obtaining the numerical solution of the incompressible Navier–Stokes equations, apart from the treatment of non-linearities, lies in the Stokes stage and specifically in the determination of the pressure field which will ensure a solenoidal velocity field. The question is how to uncouple the velocity and the pressure operators to efficiently reach an accurate solution to the unsteady Stokes problem, without degrading the predefined stability properties of the chosen scheme for the Navier–Stokes equations.

Historically, the first idea was proposed by Uzawa [1,2] and applied for numerical approximations with several methods [3,4]. It is a safe and efficient method for the numerical approximation of the Stokes problem. In complex geometries or three-dimensional domains, this method turns out to be inappropriate for its computational time cost which becomes very high. A different method is to uncouple the pressure from the velocity by means of a time splitting scheme that significantly reduces the computational cost. A large number of theoretical and numerical works have been published that discuss the accuracy and the stability properties of such methods. The most widespread methods are pressure-correction schemes. They were first introduced by Chorin-Temam [5,6], and improved by Goda (the standard incremental scheme) in [7], and later by Timmermans in [8] (the rotational incremental scheme). They require the solution of two sub-steps for each time step: the pressure is treated explicitly in the first one, and is corrected in the second one by projecting the predicted velocity onto an ad hoc space. The governing equation on the pressure or the pressure increment is a Poisson equation derived from the

* Corresponding author.
E-mail addresses: apoux@enscbp.fr (A. Poux), glockner@enscbp.fr (S. Glockner), azaiez@enscbp.fr (M. Azaïez).

0021-9991/$ - see front matter
doi:10.1016/j.jcp.2011.02.024

momentum equation by requiring incompressibility. In [9,10], the authors proved the reliability of such approaches from the stability and the convergence rate point of view. A series of numerical issues related to the analysis and implementation of fractional step methods for incompressible flows are addressed in the review paper of Guermond et al. [11]. In this reference, the authors describe the state of the art for both theoretical and numerical results related to the time splitting approach. One emerging conclusion points out that time splitting can be a high order alternative to solve the unsteady Stokes problem when the velocity boundary condition is of the Dirichlet type.

However, in many applications such as free surface problems and channel flows, one also has to deal with an outlet boundary condition on all or part of the boundary, on which the applied numerical condition should not disturb upstream flow. A large variety of this kind of boundary condition exists [12,13], such as the non-reflecting outlet boundary condition (and its adaptations) derived from a wave equation, which is suited to wake and jet flow with moderate and high Reynolds number [14–19]. Hereafter we will present some improvements on the open or traction boundary condition which is efficient for low Reynolds number and fluid–structure interactions [20–22]. The traction boundary condition was successfully used to compute various flows such as those around a circular cylinder, over a backward facing step and in a bifurcated tube [20]. Bruneau [23] proposes an evolution of the traction boundary condition involving inertial terms. Hasan [24] proposes, in the computation of incompressible flow around rigid bodies, to extrapolate velocity on the outflow boundary, pressure being obtained through traction boundary conditions.

In the case of open or traction boundary conditions, several questions remain open especially when the pressure-correction version is considered as mentioned in [10]. Indeed, Guermond et al. [11], have proven that only spatial and time convergence rates between $O(\Delta x + \Delta t)$ and $O(\Delta x^{3/2} + \Delta t^{3/2})$ on the velocity and $O(\Delta x^{1/2} + \Delta t^{1/2})$ on the pressure are to be expected with the standard incremental scheme, and between $O(\Delta x + \Delta t)$ and $O(\Delta x^{3/2} + \Delta t^{3/2})$ on the velocity and pressure for the rotational incremental scheme. Févrière [25] combines the penalty and projection methods to improve error levels of a manufactured case with open boundary conditions, but without improvement of the convergence rate. Finally, Liu [20], with a pressure Poisson equation formulation, proposes a new implementation of the open and traction boundary conditions. He proves unconditional stability with a first order time scheme and shows second order numerical convergence rate on velocity and pressure.

The aim of this paper is to propose a numerical scheme for the incompressible Navier–Stokes equations with open and traction boundary conditions, using the pressure-correction version of the time splitting methods. A new way to enforce this type of boundary condition is proposed and improves the order of convergence for both pressure and velocity. In the second part of this article we will describe the governing equations, and, in the third part, the pressure-correction schemes for open boundary conditions. In the fourth part, we will present the improvements we made on the numerical implementation of the traction and open boundary conditions. In a fifth section we will illustrate numerically the proposed method with two manufactured cases and two physical cases.

First of all we specify some notations. Let us consider a Lipschitz domain $\Omega \subset \mathbb{R}^d$, $(d = 2 \text{ or } 3)$, the generic point of Ω is denoted $\mathbf{x}$. The classical Lebesgue space of square integrable functions $L^2(\Omega)$ is endowed with the inner product:

$$(\phi, \psi) = \int_\Omega \phi\psi \; d\boldsymbol{x},$$

and the norm

$$\|\psi\|_{L^2(\Omega)} = \left(\int_\Omega |\psi(\boldsymbol{x})|^2\right)^{\frac{1}{2}}.$$

We break the time interval $[0,t^*]$ into N subdivisions of length $\Delta t = \frac{t^*}{N}$, called the time step, and define $t^n = n\Delta t$, for any n, $0 \leqslant n \leqslant N$. Let $\varphi^0, \varphi^1, \ldots, \varphi^N$ be some sequence of functions in $E = L^2$. We denote this sequence by $\varphi^{\Delta t}$, and we define the following discrete norm

$$\|\varphi^{\Delta t}\|_{l^2(E)} = \left(\Delta t \sum_{k=0}^{N} \|\varphi^k\|_E^2\right)^{\frac{1}{2}}. \tag{1.1}$$

In practice the following error estimator can be used

$$\|\varphi\|^2_{E(t^*)} = \|\varphi(\cdot, t^*)\|_E. \tag{1.2}$$

Finally, bold Latin letters like $\boldsymbol{u}$, $\boldsymbol{w}$, $\boldsymbol{f}$, etc., indicate vector valued quantities, while capitals (e.g. $\boldsymbol{X}$, etc.) are functional sets involving vector fields.

2. Governing equations

Let Ω be a regular bounded domain in $\mathbb{R}^d$ with $\boldsymbol{n}$ the unit normal to the boundary $\Gamma = \partial\Omega$ oriented outward. We suppose that Γ is partitioned into two portions Γ_D and Γ_N.

Our study consists, for a given finite time interval $[0,t^*]$ in computing velocity $\boldsymbol{u} = \boldsymbol{u}(\boldsymbol{x},t)$ and pressure $p = p(\boldsymbol{x},t)$ fields satisfying:

$$\rho\partial_t \boldsymbol{u} - \mu\Delta\boldsymbol{u} + \boldsymbol{\nabla} p = \boldsymbol{f} \quad \text{in } \Omega \times [0, t^*], \tag{2.3}$$

$$\boldsymbol{\nabla} \cdot \boldsymbol{u} = 0 \quad \text{in } \Omega \times [0, t^*], \tag{2.4}$$

$$\boldsymbol{u} = \boldsymbol{g} \quad \text{on } \Gamma_D \times [0, t^*], \tag{2.5}$$

$$(\mu\nabla\boldsymbol{u} - p\boldsymbol{Id})\boldsymbol{n} = \boldsymbol{t} \quad \text{on } \Gamma_N \times [0, t^*], \tag{2.6}$$

where ρ and μ are respectively the density and the dynamic viscosity of the flow. The body force $\boldsymbol{f} = \boldsymbol{f}(\boldsymbol{x}, t)$, the pseudo-constraint $\boldsymbol{t} = \boldsymbol{t}(\boldsymbol{x}, t)$ and the boundary condition $\boldsymbol{g} = \boldsymbol{g}(\boldsymbol{x}, t)$ are known. For sake of simplicity, we chose $\boldsymbol{g} = 0$. Finally, the initial state is characterised by a given $\boldsymbol{u}(.,0)$.

In some cases, the open or natural boundary condition (2.6) can be replaced by the traction boundary condition written as

$$\left(\mu(\nabla\boldsymbol{u} + \nabla\boldsymbol{u}^T) - p\boldsymbol{Id}\right)\boldsymbol{n} = \boldsymbol{t}. \tag{2.7}$$

3. Pressure-correction schemes for open boundary condition

We shall compute two sequences $(\boldsymbol{u}^n)_{0 \leqslant n \leqslant N}$ and $(p^n)_{0 \leqslant n \leqslant N}$ in a recurrent way that approximate in some sense the quantities $(\boldsymbol{u}(.,t^n))_{0 \leqslant n \leqslant N}$ and $(p(.,t^n))_{0 \leqslant n \leqslant N}$, solutions of the unsteady Stokes problem (2.3)–(2.6). Its semi-discrete version reads:

$$\rho\frac{\alpha\boldsymbol{u}^{n+1} + \beta\boldsymbol{u}^n + \gamma\boldsymbol{u}^{n-1}}{\Delta t} - \mu\Delta\boldsymbol{u}^{n+1} + \nabla p^{n+1} = \boldsymbol{f}^{\,n+1} \quad \text{in } \Omega, \tag{3.8}$$

$$\nabla \cdot \boldsymbol{u}^{n+1} = 0 \quad \text{in } \Omega, \tag{3.9}$$

$$\mathbf{u}^{n+1} = 0 \quad \text{on } \Gamma_D, \tag{3.10}$$

$$\left(\mu\nabla\boldsymbol{u}^{n+1} - p^{n+1}\boldsymbol{Id}\right)\boldsymbol{n} = \boldsymbol{t}^{n+1} \quad \text{on } \Gamma_N. \tag{3.11}$$

Values of parameters α, β, γ depend on the temporal scheme used. Namely:

- $\alpha = 1$, $\beta = -1$, $\gamma = 0$ for the first order Euler time scheme,
- $\alpha = \frac{3}{2},\ \beta = -2,\ \gamma = \frac{1}{2}$ for the second order Backward Difference Formulae time scheme.

Eqs. (3.8)–(3.11) are split into two subproblems. The first is the prediction diffusion problem that computes a prediction velocity fields: *find* $\boldsymbol{u}^{n+1/2}$ *such that:*

$$\rho\frac{\alpha\boldsymbol{u}^{n+1/2} + \beta\boldsymbol{u}^n + \gamma\boldsymbol{u}^{n-1}}{\Delta t} - \mu\Delta\boldsymbol{u}^{n+1/2} + \nabla p^n = \boldsymbol{f}^{\,n+1} \quad \text{in } \Omega, \tag{3.12}$$

$$\mathbf{u}^{n+1/2} = 0 \quad \text{on } \Gamma_D, \tag{3.13}$$

$$\left(\mu\nabla\boldsymbol{u}^{n+1/2} - \tilde{p}^{n+1}\boldsymbol{Id}\right)\boldsymbol{n} = \boldsymbol{t}^{n+1} \quad \text{on } \Gamma_N. \tag{3.14}$$

In the last Eq. (3.14), the expression of $\tilde{p}^{n+1}$ depends on the considered time scheme. To ensure the expected order of the time approximation, we propose two cases:

- $\alpha = 1$, $\beta = -1$, $\gamma = 0$ then $\tilde{p}^{n+1} = p^n$,
- $\alpha = \frac{3}{2},\ \beta = -2,\ \gamma = \frac{1}{2}$ then $\tilde{p}^{n+1} = 2p^n - p^{n-1}$.

The second step is a pressure-continuity correction: *find* $(\boldsymbol{u}^{n+1}, p^{n+1})$ *such that:*

$$\frac{\rho\alpha}{\Delta t}\left(\boldsymbol{u}^{n+1} - \boldsymbol{u}^{n+1/2}\right) + \nabla\varphi^{n+1} = \boldsymbol{0} \quad \text{in } \Omega, \tag{3.15}$$

$$\nabla \cdot \boldsymbol{u}^{n+1} = 0 \quad \text{in } \Omega, \tag{3.16}$$

$$\boldsymbol{u}^{n+1} \cdot \boldsymbol{n} = 0 \quad \text{on } \Gamma_D, \tag{3.17}$$

$$\text{B.C.}^{n+1} \quad \text{on } \Gamma_N. \tag{3.18}$$

and the pressure is upgraded via:

$$p^{n+1} = p^n + \varphi^{n+1} - \chi\mu\nabla \cdot \boldsymbol{u}^{n+1/2} \quad \text{in } \Omega. \tag{3.19}$$

The parameter χ is used to switch between the standard incremental scheme and the rotational one:

- $\chi = 0$ for the standard incremental scheme,

- $\chi = 0.7$ for the rotational incremental scheme[1].

The second step is rewritten as a Poisson problem on φ^{n+1}:

$$\frac{\Delta t}{\alpha\rho}\nabla\cdot\nabla\varphi^{n+1} = \nabla\cdot\boldsymbol{u}^{n+1/2} \quad \text{in } \Omega, \tag{3.20}$$

$$\frac{\partial}{\partial n}\varphi^{n+1} = 0 \quad \text{on } \Gamma_D, \tag{3.21}$$

$$\text{B.C.}^{n+1} \quad \text{on } \Gamma_N, \tag{3.22}$$

completed by:

$$p^{n+1} = p^n + \varphi^{n+1} - \chi\mu\nabla\cdot\boldsymbol{u}^{n+1/2} \quad \text{in } \Omega, \tag{3.23}$$

$$\boldsymbol{u}^{n+1} = \boldsymbol{u}^{n+1/2} - \frac{\Delta t}{\rho\alpha}\nabla\varphi^{n+1} \quad \text{in } \Omega. \tag{3.24}$$

The main result of this contribution lies in the definition of B.C.$^{n+1}$ in (3.22). As mentioned in [22] the "natural choice" which consists in considering φ^{n+1} equals zero on Γ_N leads to a kind of numerical locking for $\chi = 0$ since the boundary condition on the pressure increment causes the pressure on the limit to be equal to its initial value. The convergence of the algorithm is low and slow. To circumvent this difficulty the authors suggest to use the rotational incremental version. In the present work we propose an alternative improving the accuracy for the standard incremental version while remaining compatible with the rotational one. Indeed, the boundary condition on φ can be induced by derivation of the Helmholtz–Hodge decomposition of the $\boldsymbol{u}^{n+1/2}$ (3.15). This approach has already been followed by Brazza in [17] and Kirpatrick in [26] for other kinds of outlet boundary conditions (non-reflecting or Neumann).

4. Improvement of the pressure boundary conditions

For the sake of simplicity we choose Ω to be a square and we fix Γ_N at its right boundary. The starting point of our approach is the first component of Eq. (3.15) that we derive on x_1:

$$-\frac{\Delta t}{\alpha\rho}\partial_{x_1^2}\varphi^{n+1} = \partial_{x_1}u_{x_1}^{n+1} - \partial_{x_1}u_{x_1}^{n+\frac{1}{2}}. \tag{4.25}$$

We project Eqs. (3.11) and (3.14) on direction x_1:

$$\mu\partial_{x_1}u_{x_1}^{n+1} - p^{n+1} = t_{x_1}^{n+1}, \tag{4.26}$$

$$\mu\partial_{x_1}u_{x_1}^{n+\frac{1}{2}} - \tilde{p}^{n+1} = t_{x_1}^{n+1}, \tag{4.27}$$

and combining those three equations, one can verify that (4.25) is equivalent to:

$$-\frac{\Delta t}{\alpha\rho}\partial_{x_1^2}\varphi^{n+1} = \frac{1}{\mu}(p^{n+1} - \tilde{p}^{n+1}). \tag{4.28}$$

Depending on the choice of the time splitting version and the time order scheme, $p^{n+1} - \tilde{p}^{n+1}$ can be replaced by its approximation expression using φ^{n+1} and the divergence of the predicted velocity. For the first order time scheme, we easily derive the following boundary conditions:

$$\left(\frac{\Delta t}{\alpha\rho}\partial_{x_1^2} + \frac{1}{\mu}\right)\varphi^{n+1} = \chi\nabla\cdot\boldsymbol{u}^{n+\frac{1}{2}}. \tag{4.29}$$

Or, for a second order scheme:

$$\left(\frac{\Delta t}{\alpha\rho}\partial_{x_1^2} + \frac{1}{\mu}\right)\varphi^{n+1} = \frac{\varphi^n}{\mu} + \chi\nabla\cdot\left(\boldsymbol{u}^{n+\frac{1}{2}} - \boldsymbol{u}^{n-\frac{1}{2}}\right). \tag{4.30}$$

Subtracting (4.29) or (4.30) in (3.20) leads to a version that is easier to implement:

- First-order open boundary condition (OBC1):

$$\left(\frac{\Delta t}{\alpha\rho}\partial_{x_2^2} - \frac{1}{\mu}\right)\varphi^{n+1} = (1-\chi)\nabla\cdot\boldsymbol{u}^{n+\frac{1}{2}}. \tag{4.31}$$

[1] Ideally, $\chi = 1$ but as Guermond proved in [22], for stability issues, χ is necessarily strictly less than $2\mu/d$.

- Second-order open boundary condition (OBC2):

$$\left(\frac{\Delta t}{\alpha\rho}\partial_{x_2^2}-\frac{1}{\mu}\right)\varphi^{n+1}=(1-\chi)\nabla\cdot\boldsymbol{u}^{n+\frac{1}{2}}-\frac{\varphi^n}{\mu}+\chi\nabla\cdot\boldsymbol{u}^{n-\frac{1}{2}}. \tag{4.32}$$

In summary, our approach differs from the usual one by the definition of the boundary condition on Γ_N in the correction step.

We end this section by describing the extension of (4.31) and (4.32) to a more general partition of the boundary $\partial\Omega$.

4.1. Generalisation of the boundary condition

Extension to a more general definition of Γ_N requires new notations to be introduced. Let us denote by $\boldsymbol{D}(\boldsymbol{u}) = (\nabla\boldsymbol{u} + \nabla\boldsymbol{u}^T)/2$, the rate of deformation tensor and $\boldsymbol{\sigma}(\boldsymbol{u},p) = -p\boldsymbol{Id} + 2\mu\boldsymbol{D}$ the stress one. $\boldsymbol{n}$ and $\boldsymbol{\tau}$ are respectively the units normal to the boundary oriented outward and the associated unit tangent vector.

The traction boundary condition $\boldsymbol{\sigma}(\boldsymbol{u},p)$: $\boldsymbol{n} = \boldsymbol{t}$ projected on $\boldsymbol{n}$ and $\boldsymbol{\tau}$ is written:

$$2\mu\boldsymbol{D}(\boldsymbol{u}^{n+1}):\boldsymbol{n}\cdot\boldsymbol{n}-p^{n+1}=\boldsymbol{t}^{n+1}\cdot\boldsymbol{n}, \tag{4.33}$$

$$2\mu\boldsymbol{D}(\boldsymbol{u}^{n+1}):\boldsymbol{n}\cdot\boldsymbol{\tau}.=\boldsymbol{t}^{n+1}\cdot\boldsymbol{\tau}. \tag{4.34}$$

Applying $\boldsymbol{D}$ to (3.15) gives us:

$$\boldsymbol{D}(\boldsymbol{u}^{n+1})-\boldsymbol{D}\left(\boldsymbol{u}^{n+\frac{1}{2}}\right)=-\frac{\Delta t}{\alpha\rho}\boldsymbol{D}(\nabla\varphi^{n+1}). \tag{4.35}$$

Denoting $\boldsymbol{L}(\varphi^{n+1}) = \boldsymbol{D}(\nabla\varphi^{n+1})$, we have:

$$\boldsymbol{D}(\boldsymbol{u}^{n+1}):\boldsymbol{n}\cdot\boldsymbol{n}-\boldsymbol{D}\left(\boldsymbol{u}^{n+\frac{1}{2}}\right):\boldsymbol{n}\cdot\boldsymbol{n}=-\frac{\Delta t}{\alpha\rho}\boldsymbol{L}(\varphi^{n+1}):\boldsymbol{n}\cdot\boldsymbol{n}. \tag{4.36}$$

Using (4.33) and (3.23) we obtain:

$$-\frac{\Delta t}{\alpha\rho}\boldsymbol{L}(\varphi^{n+1}):\boldsymbol{n}\cdot\boldsymbol{n}=\frac{\boldsymbol{t}^{n+1}\cdot\boldsymbol{n}+p^n+\varphi^{n+1}-\chi\mu\nabla\cdot\boldsymbol{u}^{n+\frac{1}{2}}}{2\mu}-\boldsymbol{D}\left(\boldsymbol{u}^{n+\frac{1}{2}}\right):\boldsymbol{n}\cdot\boldsymbol{n}.$$

Thus, for the first order boundary condition, we can impose on $(\boldsymbol{u}^{n+\frac{1}{2}},\varphi^{n+1})$:

$$2\mu\boldsymbol{D}\left(\boldsymbol{u}^{n+\frac{1}{2}}\right):\boldsymbol{n}\cdot\boldsymbol{n}=\boldsymbol{t}^{n+1}\cdot\boldsymbol{n}+p^n, \tag{4.37}$$

$$2\mu\boldsymbol{D}\left(\boldsymbol{u}^{n+\frac{1}{2}}\right):\boldsymbol{n}\cdot\boldsymbol{\tau}=\boldsymbol{t}^{n+1}\cdot\boldsymbol{\tau}, \tag{4.38}$$

$$\frac{\Delta t}{\alpha\rho}\boldsymbol{L}(\varphi^{n+1}):\boldsymbol{n}\cdot\boldsymbol{n}+\frac{\varphi^{n+1}}{2\mu}=\frac{\chi}{2}\nabla\cdot\boldsymbol{u}^{n+\frac{1}{2}}. \tag{4.39}$$

Or, to have second order scheme:

$$2\mu\boldsymbol{D}\left(\boldsymbol{u}^{n+\frac{1}{2}}\right):\boldsymbol{n}\cdot\boldsymbol{n}=\boldsymbol{t}^{n+1}\cdot\boldsymbol{n}+2p^n-p^{n-1}, \tag{4.40}$$

$$2\mu\boldsymbol{D}\left(\boldsymbol{u}^{n+\frac{1}{2}}\right):\boldsymbol{n}\cdot\boldsymbol{t}=\boldsymbol{t}^{n+1}\cdot\boldsymbol{\tau}, \tag{4.41}$$

$$\frac{\Delta t}{\alpha\rho}\boldsymbol{L}(\varphi^{n+1}):\boldsymbol{n}\cdot\boldsymbol{n}+\frac{\varphi^{n+1}}{2\mu}=\frac{\varphi^n}{2\mu}+\frac{\chi}{2}\nabla\cdot\left(\boldsymbol{u}^{n+\frac{1}{2}}-\boldsymbol{u}^{n-\frac{1}{2}}\right). \tag{4.42}$$

To conclude this section, the full time-splitting algorithm in the presence of traction boundary conditions reads:

Prediction step. *Find $\boldsymbol{u}^{n+1/2}$ such that:*

$$\rho\frac{\alpha\boldsymbol{u}^{n+1/2}+\beta\boldsymbol{u}^n+\gamma\boldsymbol{u}^{n-1}}{\Delta t}-\mu\Delta\boldsymbol{u}^{n+1/2}+\nabla p^n=\boldsymbol{f}^{\,n+1},\quad \text{in } \Omega, \tag{4.43}$$

$$\mathbf{u}^{n+1/2}=0,\quad \text{on } \Gamma_D, \tag{4.44}$$

$$\left(\mu\left(\nabla\boldsymbol{u}^{n+1/2}+(\nabla\boldsymbol{u}^{n+1/2})^T\right)-\tilde{p}^{n+1}\boldsymbol{Id}\right)\boldsymbol{n}=\boldsymbol{t}^{n+1}\quad \text{on } \Gamma_N. \tag{4.45}$$

Correction pressure-continuity step. *Find* $(\boldsymbol{u}^{n+1}, p^{n+1})$ *such that:*

$$\frac{\Delta t}{\alpha\rho}\nabla\cdot\nabla\varphi^{n+1} = \nabla\cdot\boldsymbol{u}^{n+1/2} \quad \text{in } \Omega, \tag{4.46}$$

$$\frac{\partial}{\partial n}\varphi^{n+1} = 0 \quad \text{on } \Gamma_D, \tag{4.47}$$

$$\frac{\Delta t}{\alpha\rho}\boldsymbol{L}(\varphi^{n+1}) : \boldsymbol{n}\cdot\boldsymbol{n} + \frac{\varphi^{n+1}}{2\mu} = \frac{\chi}{2}\nabla\cdot\boldsymbol{u}^{n+\frac{1}{2}} + \gamma\left(\frac{\varphi^n}{\mu} - \chi\nabla\cdot\boldsymbol{u}^{n-\frac{1}{2}}\right), \quad \text{on } \Gamma_N. \tag{4.48}$$

Completed by:

$$p^{n+1} = p^n + \varphi^{n+1} - \chi\mu\nabla\cdot\boldsymbol{u}^{n+1/2} \quad \text{in } \Omega, \tag{4.49}$$

$$\boldsymbol{u}^{n+1} = \boldsymbol{u}^{n+1/2} - \frac{\Delta t}{\rho\alpha}\nabla\varphi^{n+1} \quad \text{in } \Omega. \tag{4.50}$$

The choice of χ permits us to switch from the standard incremental scheme ($\chi = 0$) to the rotational form $\left(\chi < \frac{2\mu}{d}\right)$ while the values of α, β, γ move from the first time order to the second:

- $\alpha = 1$, $\beta = -1$, $\gamma = 0$ for first order Euler time scheme; then $\tilde{p}^{n+1} = p^n$,
- $\alpha = \frac{3}{2}$, $\beta = -2$, $\gamma = \frac{1}{2}$ for second order Backward Difference Formulae time scheme; then $\tilde{p}^{n+1} = 2p^n - p^{n-1}$.

5. Numerical experiments

We start this section by giving a brief description of the space discretisation and tools for the numerical simulations. Then, numerical experiments involving the proposed boundary conditions are separated into verification cases on manufactured solutions of the Stokes equations, and validation on physical cases governed by the Navier–Stokes equations.

5.1. Spatial discretisation and linear solvers

Spatial discretisation is based on the finite volume method. To avoid the well known spurious modes phenomena, the correction step uses the stable finite volume staggered grid of the Marker and Cells type [27]. In our implementation, pressure unknowns are associated to the cell vertices whereas velocity components are face centred. The approximation of the prediction-diffusion of the Stokes problem step uses a centred scheme of second order to compute the predicted velocity. The approach adopted for the treatment of the Navier–Stokes non-linear term $(\boldsymbol{u}\cdot\nabla)\boldsymbol{u}$ involved in the material derivative of the velocity consists in linearising it by $((2\boldsymbol{u}^{\boldsymbol{n}} - \boldsymbol{u}^{\boldsymbol{n}-1}).\nabla)\boldsymbol{u}^{n+1}$ and applying a second-order centred scheme.

In the following simulations, the proposed boundary condition (4.48), which contains high order derivatives in the normal direction of the boundary, is treated by subtracting it in (3.20) which leads to a formulation involving only tangential derivatives. As pressure unknowns are associated to the cell vertices, these derivatives are trivial to discretise by a second-order centred scheme. This approach would be valid for any orthogonal curvilinear coordinate system.

All the computations are made using the parallel version of a Navier–Stokes solver based on the block-structured mesh partitioner described in [28]. Finally and in order to solve the linear systems we are using:

- For the prediction step, the iterative BiCGStab method with a point Jacobi preconditioner of the HYPRE library [29].
- For the correction step, the multifrontal sparse direct solver MUMPS [30] for manufactured cases or the GMRES method with a semi-coarsening geometric multigrid preconditioner [31,32] of the HYPRE library for physical cases.

5.2. Numerical results for the Stokes problem

To assess the error convergence rate of the methods in space and time, we consider two manufactured test cases with $\rho = 1$ and $\mu = 1$. The domain is chosen to be $\Omega = [-1;1]^2$ and we enforce the traction boundary condition on the right part of the box and a Dirichlet boundary condition everywhere else. Exact solutions for $\boldsymbol{u}^{ex} = (u^{ex}_{x_1}, u^{ex}_{x_2})$ and p^{ex} are:

- For the homogeneous case ($\boldsymbol{t} = \boldsymbol{0}$):

$$u^{ex}_{x_1} = \sin(x_1)\sin(x_2)\cos(2\pi\omega t),$$
$$u^{ex}_{x_2} = \cos(x_1)\cos(x_2)\cos(2\pi\omega t),$$
$$p^{ex} = -2\cos(1)\sin(2(x_1 - 1) - x_2)\cos(2\pi\omega t).$$

- For the non-homogeneous case, we take the same problem as [20]:

$$u_{x_1}^{ex} = \cos^2\left(\frac{\pi x_1}{4}\right)\sin\left(\frac{\pi x_2}{2}\right)\cos(2\pi\omega t),$$
$$u_{x_2}^{ex} = -\cos^2\left(\frac{\pi x_2}{4}\right)\sin\left(\frac{\pi x_1}{2}\right)\cos(2\pi\omega t),$$
$$p^{ex} = \cos\left(\frac{\pi x_1}{4}\right)\sin\left(\frac{\pi x_2}{4}\right)\cos(2\pi\omega t).$$

We present hereafter a convergence study with a traction boundary condition, homogeneous or not. The error estimator $\|\varphi\|^2_{L^2(t^*)}$ defined in (1.2) is used.

5.2.1. Error convergence rate in space

Most of the research effort made on pressure-correction methods deals with the time convergence rate, since optimal space one can be reached in presence of Dirichlet boundary conditions on velocity. Nevertheless, in open or traction boundary conditions, spatial convergence rates are limited to Δx for velocity and $O(\Delta x^{1/2})$ for pressure. The only known way to overcome this difficulty in the framework of pressure-correction methods is to switch to the rotational formulation.

In order to study the spatial splitting error we carried out the first numerical experiment with $\omega = 0$. The time step is fixed at $\Delta t = 10^{-3}$ and we run the algorithm for different values of Δx. Stationary tolerance is set to 10^{-12}. As long as we attempt to approximate analytical solutions by a second order scheme, we expect that the errors decay like Δx^2. The representative curves of Figs. 1 and 2 (on the left) show that the convergence rate of the error on the velocity and the pressure are $O(\Delta x^2)$. We obtain exactly the same result with the first and the second order (in time) versions.

Repeating these tests with the rotational scheme, we obtain a $O(\Delta x^2)$ convergence rate of the error on velocity and pressure whatever the method used (see Figs. 1 and 2 on the right).

As a conclusion on the spatial convergence rate, we can say that the proposed method improves the standard incremental scheme from $O(\Delta x)$ to $O(\Delta x^2)$ for the velocity and from $O(\Delta x^{1/2})$ to $O(\Delta x^2)$ for pressure, while remaining compatible with the rotational scheme. The question now is to know if the numerical locking of the incremental scheme also observed for the error convergence rate in time is overcome, and if the method is still compatible with the rotational formulation.

5.2.2. Error convergence rate in time

To study the time splitting error, we consider the unsteady case $\omega = 1$. In Figs. 3 and 4 we plotted for Δx fixed at 1/256 and for a range of time steps $10^{-4} \leqslant \Delta t \leqslant 10^{-1}$ the errors (1.2) at $t = 2$. With the first order proposed boundary condition, the convergence rate of the error on the velocity and the pressure are around $O(\Delta t)$. While with the second order boundary condition we ensure a convergence rate of $O(\Delta t^2)$, for the velocity and between $O(\Delta t^{3/2})$ and $O(\Delta t^2)$ for pressure. Thus, the convergence rate in the presence of an open or traction boundary condition is now brought to the level observed with the Dirichlet boundary condition.

We repeated these tests with the rotational scheme. As one can see in Figs. 5 and 6, for the standard boundary condition ($\varphi = 0$ on Γ_N) the convergence rate of the error on the velocity and the pressure is between $O(\Delta t^{3/2})$ and $O(\Delta t^2)$, which are the same as [22]. With the proposed first order boundary condition, the convergence rate of the error on the velocity and the pressure is around $O(\Delta t)$. And finally, with the second order boundary condition we can obtain a clear convergence rate of the error on the velocity of $O(\Delta t^2)$ and on the pressure of $O(\Delta t^2)$.

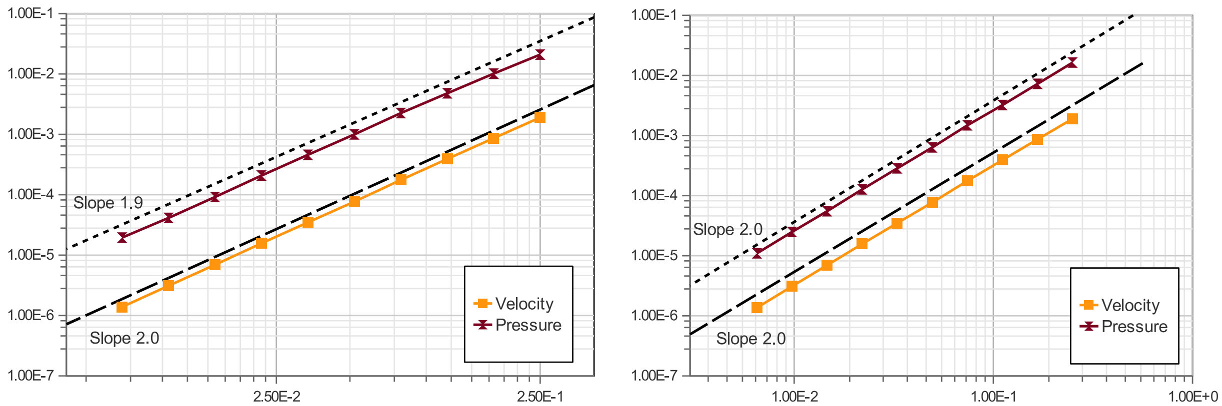

Fig. 1. Spatial convergence rates with the standard incremental scheme (left) and the rotational scheme (right) with $\Delta t = 10^{-3}$ for the steady homogeneous case.

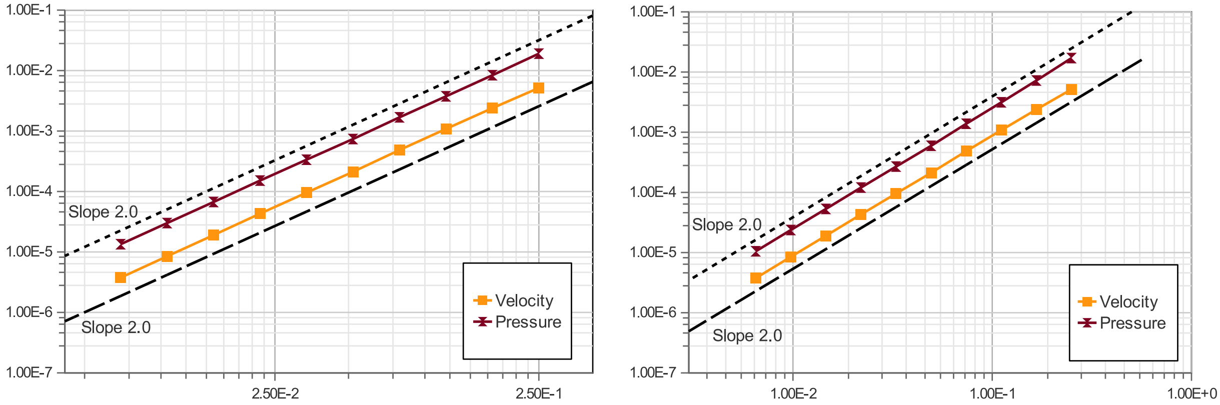

Fig. 2. Spatial convergence rates with the standard incremental scheme (left) and the rotational scheme (right) with $\Delta t = 10^{-3}$ for the steady non-homogeneous case.

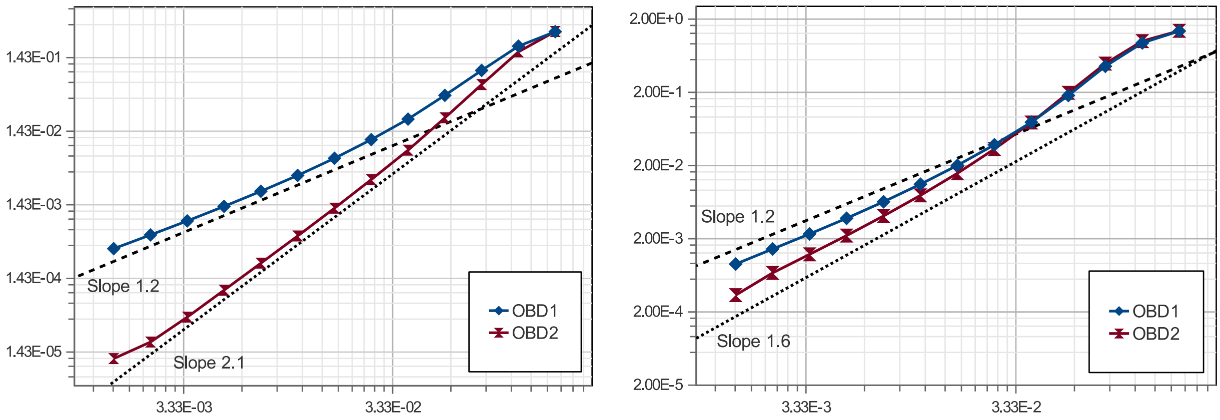

Fig. 3. Time convergence rates with the standard incremental scheme at $t = 2$ with $\Delta x = 1/256$ for the unsteady homogeneous case. Velocity (left) and pressure (right).

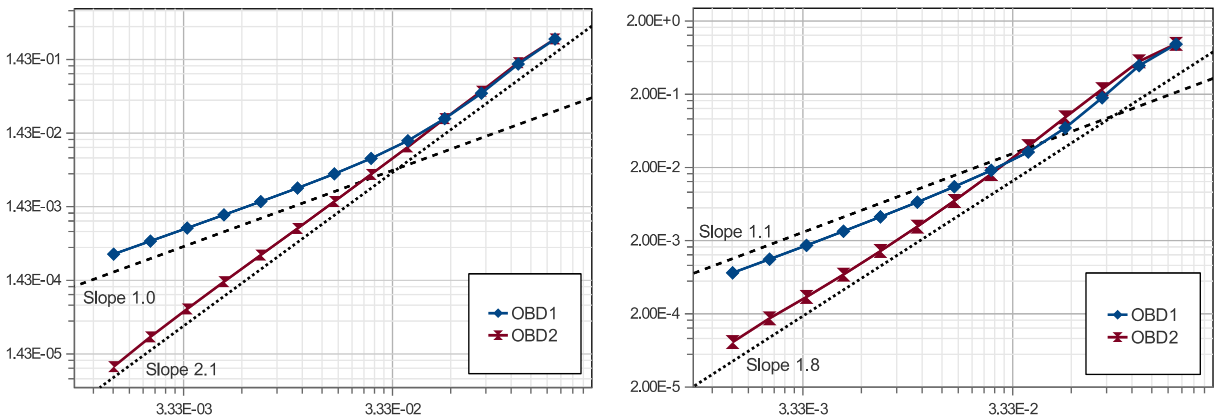

Fig. 4. Time convergence rates with the standard incremental scheme at $t = 2$ with $\Delta x = 1/256$ for the unsteady non-homogeneous case. Velocity (left) and pressure (right).

Remark 1. In Figs. 5 and 6 (right) there is a saturation of the time error by space error at small time step due to space discretisation being too coarse. This behaviour is illustrated in Fig. 7 which represents the time convergence for two meshes. We can see that the finest the mesh is the more saturation is postponed to a smaller time step.

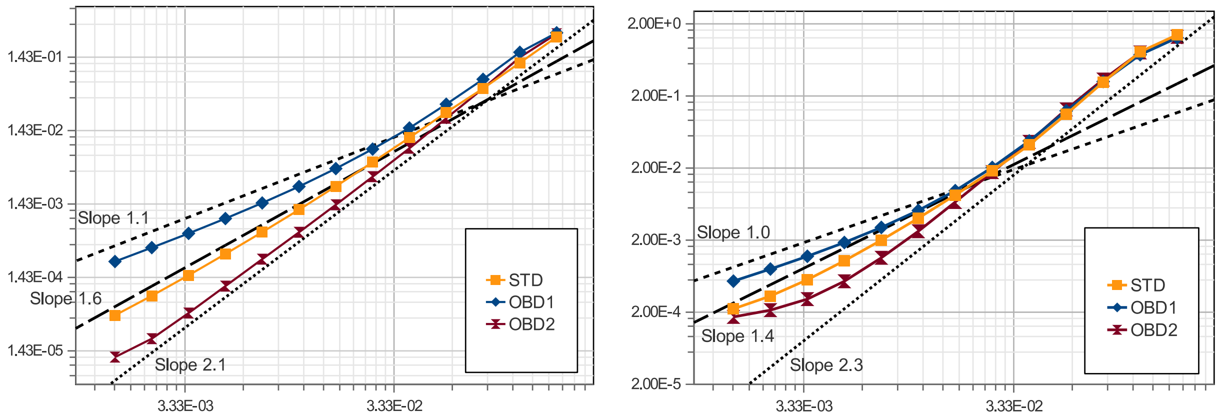

Fig. 5. Time convergence rates with the rotational incremental scheme at $t = 2$ with $\Delta x = 1/256$ for the unsteady homogeneous case. Velocity (left) and pressure (right).

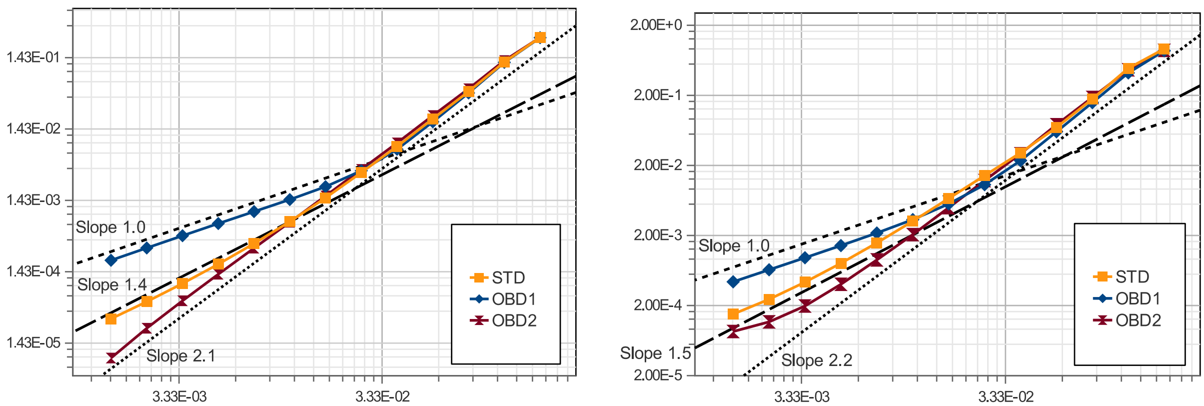

Fig. 6. Time convergence rates with the rotational incremental scheme at $t = 2$ with $\Delta x = 1/256$ for the unsteady non-homogeneous case. Velocity (left) and pressure (right).

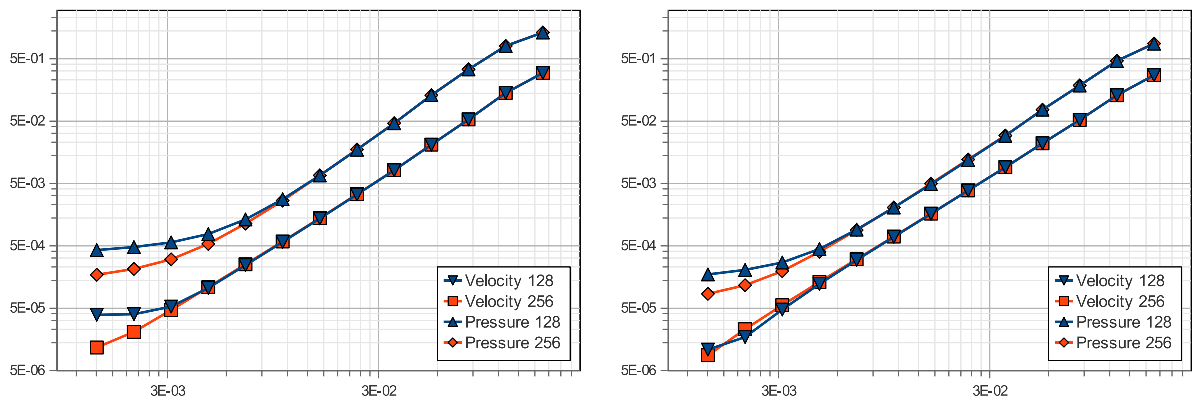

Fig. 7. Time convergence rates for the unsteady homogeneous case (left) and non-homogeneous case (right) with the rotational incremental scheme and OBD2 at $t = 2$ with $\Delta x = 1/128$, $\Delta x = 1/256$.

Remark 2. With Dirichlet boundary conditions on all boundaries, rotational scheme improves error level, compared to standard incremental one, while convergence order remains the same. With the standard traction boundary conditions ($\varphi = 0$ on Γ_N), we can note that rotational scheme improves convergence order. With the proposed method, a more usual effect of the rotational methods which improves only error levels is noted. This can be verified in Figs. 8 and 9.

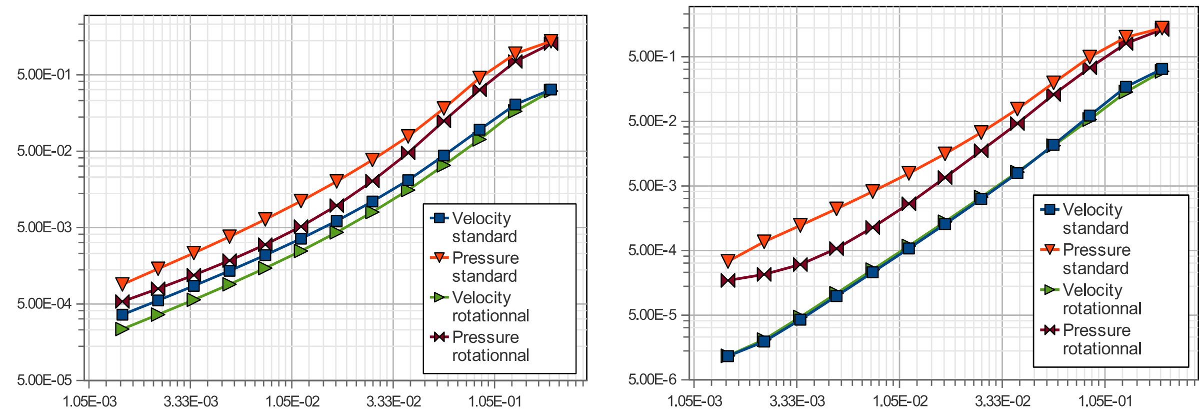

Fig. 8. Comparison between convergence rates with the rotational incremental scheme and the standard incremental scheme at $t = 2$ with $\Delta x = 1/256$ for the unsteady homogeneous case. First order (left) and second order (right) boundary conditions.

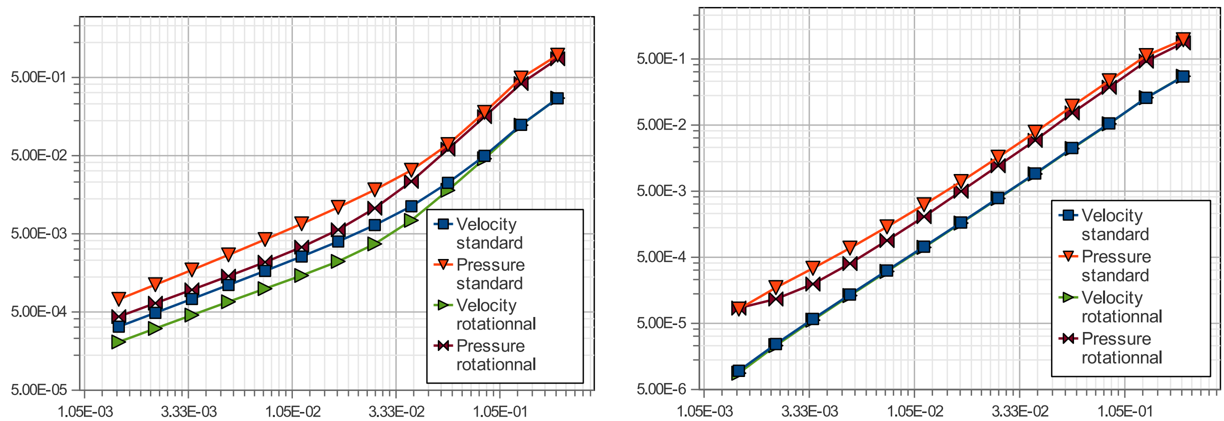

Fig. 9. Comparison between convergence rates with the rotational incremental scheme and the standard incremental scheme at $t = 2$ with $\Delta x = 1/256$ for the unsteady homogeneous case. First order (left) and second order (right) boundary conditions.

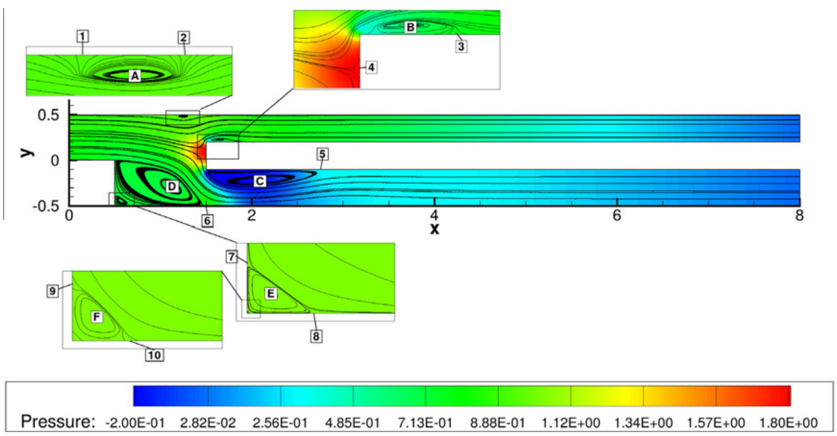

Fig. 10. Steady state of the bifurcation case. Pressure and streamlines. Eddies are numbered with letters.

Remark 3. A similar study was carried out with the open boundary condition (homogeneous or not); the norm $\|\varphi^{\Delta t}\|_{l^2(E)}$ (see (1.1)) was also used. Since the results lead to the same conclusions, they are not shown here.

Table 1
Details of some parameters in the bifurcated tube for different meshes.

Space step size (m)	0.02	0.01	0.005	0.0025	0.00125
Total kinetic energy ($kg \cdot m \cdot s^{-2}$)	$2.0142 \times 10^{+00}$	$2.0025 \times 10^{+00}$	$1.9965 \times 10^{+00}$	$1.9937 \times 10^{+00}$	$1.9923 \times 10^{+00}$
Top outflux ($m^2 \cdot s^{-1}$)	1.9803×10^{-01}	1.9623×10^{-01}	1.9505×10^{-01}	1.9443×10^{-01}	1.9410×10^{-01}
Bottom outflux ($m^2 \cdot s^{-1}$)	3.0117×10^{-01}	3.0357×10^{-01}	3.0490×10^{-01}	3.0556×10^{-01}	3.0589×10^{-01}
Top charge drop ($m^3 \cdot s^{-2}$)	4.2338×10^{-01}	4.1251×10^{-01}	4.0639×10^{-01}	4.0309×10^{-01}	4.0131×10^{-01}
Bottom charge drop ($m^3 \cdot s^{-2}$)	4.2223×10^{-01}	4.1189×10^{-01}	4.0607×10^{-01}	4.0292×10^{-01}	4.0123×10^{-01}

Table 2
Extrapolation of some parameters in the bifurcated tube.

	Extrapolated value	Extrapolation order
Total kinetic energy ($kg \cdot m \cdot s^{-2}$)	$1.9909 \times 10^{+00}$	1.07
Top outflux ($m^2 \cdot s^{-1}$)	1.9374×10^{-01}	0.92
Bottom outflux ($m^2 \cdot s^{-1}$)	3.0623×10^{-01}	1.01
Top charge drop ($m^3 \cdot s^{-2}$)	3.9924×10^{-01}	0.89
Bottom charge drop ($m^3 \cdot s^{-2}$)	3.9925×10^{-01}	0.89

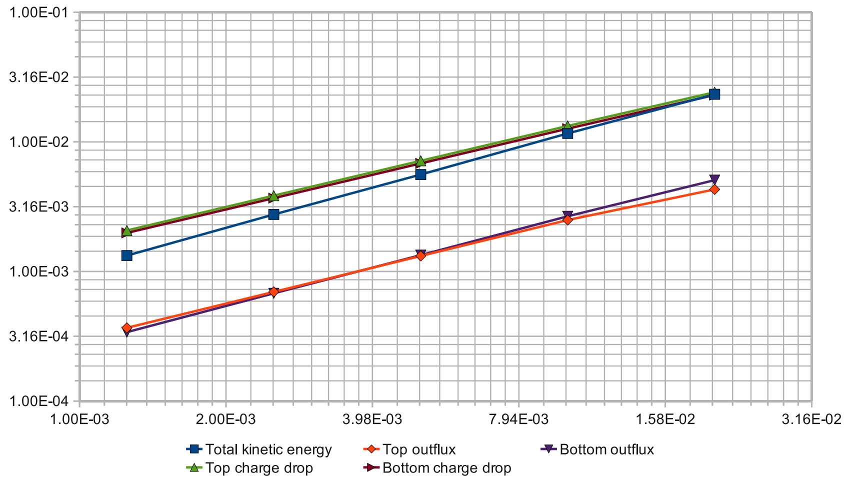

Fig. 11. Spatial convergence rates based on the extrapolation.

As a conclusion on the error convergence rate in time, the proposed method improves orders of the standard incremental scheme from $O(\Delta t)$ to $O(\Delta t^2)$ for the velocity and from $O(\Delta t^{1/2})$ to between $O(\Delta t^{3/2})$ and $O(\Delta t^2)$ for pressure. It also slightly improves the rotational scheme to a clear convergence rate of $O(\Delta t^2)$ for velocity and pressure.

5.3. Numerical results for the Navier–Stokes flows

The boundary conditions proposed are tested with two laminar incompressible physical problems: the steady flow in a bifurcated tube proposed recently by [20] and the unsteady flow past a square section cylinder (see [24,33–36]). The rotational scheme is used with second order time discretisation.

5.3.1. Flow in a bifurcated tube

We deal with the Navier–Stokes equation set on the domain shown in the Fig. 10:

$$\Omega = [0,8] \times [-0.5,0.5] \setminus \{[0,0.5] \times [-0.5,0] \cup [1.5,8] \times [-0.1,0.2]\}.$$

The inflow boundary at $\{x_1 = 0\text{m}\}$ is a Dirichlet one set to a Poiseuille flow with a unitary influx. The two outflow boundaries at $\{x_1 = 8\text{m}\}$ are the proposed open boundary condition OBC2, the remaining boundaries being the no-slip condition. Initialisation is made with $\boldsymbol{u}^0 = \boldsymbol{0}$ and $p^0 = 0$.

Fig. 10 shows steady state for $Re = 600$ based on the height of the larger section ($\rho = 1$ kg m^{-3} and $\nu = 1/600$ m^2 s^{-1}). The flow is composed by six eddies. An infinite series of Moffatt corner vortices (D, E, F) of increasingly smaller amplitude (see

Table 3
Details of eddies characteristics in the bifurcated tube for different meshes.

Δx(m)	0.02	0.01	0.005	0.0025	0.00125
Eddy A x	$1.2512 \times 10^{+0}$	$1.2534 \times 10^{+0}$	$1.2574 \times 10^{+0}$	$1.2594 \times 10^{+0}$	$1.2606 \times 10^{+0}$
Eddy A y	4.7816×10^{-1}	4.7686×10^{-1}	4.7756×10^{-1}	4.7362×10^{-1}	4.7306×10^{-1}
Eddy A ω	5.6036×10^{-1}	6.0344×10^{-1}	6.8107×10^{-1}	7.0257×10^{-1}	7.1643×10^{-1}
Point 1 x	$1.2000 \times 10^{+0}$	$1.1200 \times 10^{+0}$	$1.0850 \times 10^{+0}$	$1.0675 \times 10^{+0}$	$1.0600 \times 10^{+0}$
Point 2 x	$1.3000 \times 10^{+0}$	$1.3400 \times 10^{+0}$	$1.3600 \times 10^{+0}$	$1.3725 \times 10^{+0}$	$1.3763 \times 10^{+0}$
Eddy B x	$1.6449 \times 10^{+0}$	$1.6258 \times 10^{+0}$	$1.6234 \times 10^{+0}$	$1.6225 \times 10^{+0}$	$1.6219 \times 10^{+0}$
Eddy B y	2.2609×10^{-1}	2.2516×10^{-1}	2.2237×10^{-1}	2.2070×10^{-1}	2.1971×10^{-1}
Eddy B ω	$-8.4218 \times 10^{+0}$	$-1.0078 \times 10^{+1}$	$-9.1216 \times 10^{+0}$	$-8.5552 \times 10^{+0}$	$-8.2187 \times 10^{+0}$
Point 3 x	$1.7600 \times 10^{+0}$	$1.8100 \times 10^{+0}$	$1.8200 \times 10^{+0}$	$1.8175 \times 10^{+0}$	$1.8163 \times 10^{+0}$
Point 4 y	1.0000×10^{-1}	1.0000×10^{-1}	1.0000×10^{-1}	1.0000×10^{-1}	9.8750×10^{-2}
Eddy C x	$2.1183 \times 10^{+0}$	$2.0945 \times 10^{+0}$	$2.0844 \times 10^{+0}$	$2.0803 \times 10^{+0}$	$2.0781 \times 10^{+0}$
Eddy C y	-2.1844×10^{-1}	-2.1645×10^{-1}	-2.1498×10^{-1}	-2.1406×10^{-1}	-2.1336×10^{-1}
Eddy C ω	$1.0540 \times 10^{+1}$	$1.0180 \times 10^{+1}$	$9.9620 \times 10^{+0}$	$9.8574 \times 10^{+0}$	$9.8142 \times 10^{+0}$
Point 5 x	$2.7800 \times 10^{+0}$	$2.7900 \times 10^{+0}$	$2.7950 \times 10^{+0}$	$2.7975 \times 10^{+0}$	$2.7975 \times 10^{+0}$
Eddy D x	$1.1225 \times 10^{+0}$	$1.1340 \times 10^{+0}$	$1.1384 \times 10^{+0}$	$1.1402 \times 10^{+0}$	$1.1410 \times 10^{+0}$
Eddy D y	-2.9328×10^{-1}	-2.9682×10^{-1}	-2.9818×10^{-1}	-2.9874×10^{-1}	-2.9899×10^{-1}
Eddy D ω	$-2.7661 \times 10^{+0}$	$-2.7885 \times 10^{+0}$	$-2.7943 \times 10^{+0}$	$-2.7949 \times 10^{+0}$	$-2.7946 \times 10^{+0}$
Point 6 x	$1.4400 \times 10^{+0}$	$1.4700 \times 10^{+0}$	$1.4700 \times 10^{+0}$	$1.4725 \times 10^{+0}$	$1.4750 \times 10^{+0}$
Eddy E x	5.6857×10^{-1}	5.6466×10^{-1}	5.6229×10^{-1}	5.6094×10^{-1}	5.6023×10^{-1}
Eddy E y	-4.4269×10^{-1}	-4.4493×10^{-1}	-4.4646×10^{-1}	-4.4729×10^{-1}	-4.4723×10^{-1}
Eddy E ω	2.9552×10^{-2}	2.6039×10^{-2}	2.4409×10^{-2}	2.3540×10^{-2}	2.3088×10^{-2}
Point 7 y	-3.8000×10^{-1}	-3.8000×10^{-1}	-3.8000×10^{-1}	-3.8000×10^{-1}	-3.8000×10^{-1}
Point 8 x	6.6000×10^{-1}	6.6000×10^{-1}	6.6500×10^{-1}	6.6500×10^{-1}	6.6375×10^{-1}
Eddy F x	–	–	–	5.0269×10^{-1}	5.0316×10^{-1}
Eddy F y	–	–	–	-4.9732×10^{-1}	-4.9684×10^{-1}
Eddy F ω	–	–	–	-6.5702×10^{-5}	-1.3642×10^{-4}
Point 9 y	–	–	–	-4.9500×10^{-1}	-4.9375×10^{-1}
Point 10 x	–	–	–	5.0500×10^{-1}	5.0625×10^{-1}

[37]) appears in the lower left corner due to the sudden expansion of the section. Three other recirculations (A, B, C) are attached to the horizontal walls due to the contraction of the section. The outflux are equal to $0.194\ \mathrm{m}^2\,\mathrm{s}^{-1}$ on top and $0.306\ \mathrm{m}^2\,\mathrm{s}^{-1}$ on bottom, which are qualitatively the same as in [20] where an open boundary condition has also been used.

In order to propose a reference solution, we compute three other parameters characterising the flow:

- The total kinetic energy

$$e_c = \int_\Omega \frac{1}{2}\rho \boldsymbol{u}^2\ d\boldsymbol{x}.$$

- The outflux

$$Q = \int_R \boldsymbol{u} \cdot \boldsymbol{n}\ dl.$$

- The charge drops

$$\Delta h = \frac{1}{2}\left(\int_L (\boldsymbol{u} \cdot \boldsymbol{n})^2\ dl - \int_R (\boldsymbol{u} \cdot \boldsymbol{n})^2\ dl\right) + \frac{1}{\rho}\left(\int_L p\ dl - \int_R p\ dl\right),$$

  where L is the left boundary condition, and R the upper or lower right one.

Richardson extrapolation framework [38,39] is used to compute the convergence rates and extrapolated values of these parameters computed on four meshes of step size h_1, h_2, h_3 and h_4 verifying consecutive ratio equal to two. The convergence rate α and the extrapolated value f_{ext} are given by:

$$\alpha = \frac{\ln\left(\frac{f_{h_1} - f_{h_3}}{f_{h_2} - f_{h_4}}\right)}{\ln\left(\frac{h_1}{h_2}\right)}, \tag{5.51}$$

$$f_{\mathrm{ext}} = \frac{\left(\frac{h_3}{h_4}\right)^\alpha f_{h_4} - f_{h_3}}{\left(\frac{h_3}{h_4}\right)^\alpha - 1}. \tag{5.52}$$

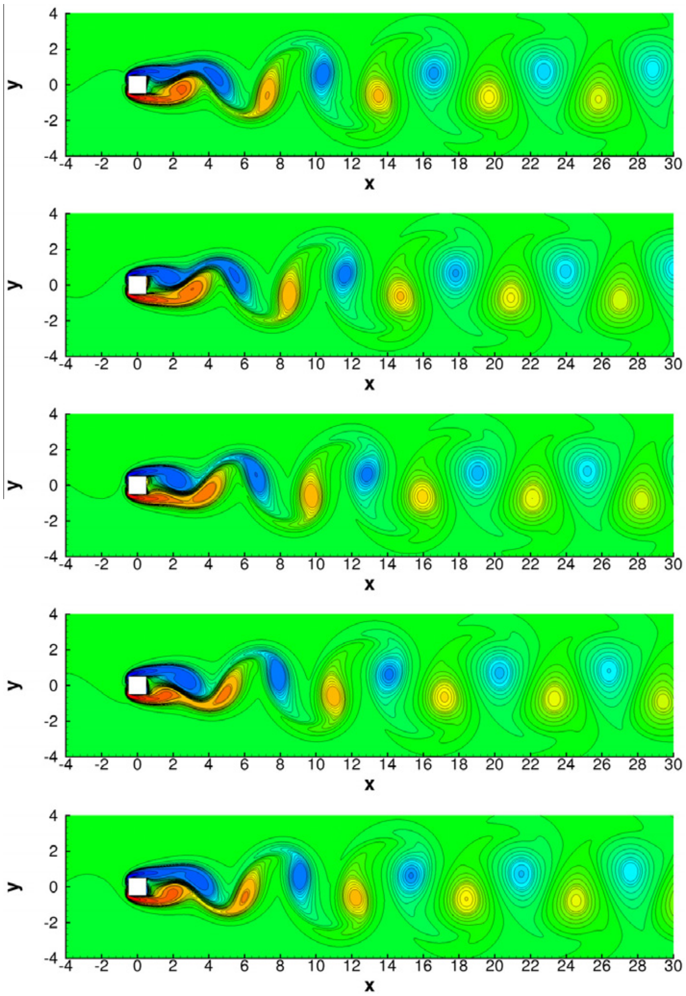

Fig. 12. Vorticity contours during one period.

Table 4
Comparison of computed flow metrics.

References	St	Average C_D	r.m.s C_L
Present study, Ω_1, 6H	0.143235	1.461515	0.153056
Present study, Ω_2, 10H	0.146412	1.474955	0.144166
Present study, Ω_3, 20H	0.147131	1.478540	0.142870
Present study, Ω_4, 30H	0.147167	1.478745	0.142652
Sohankar [34]	0.146	1.46	0.139
Pavlov [36]	0.150	1.51	0.137
Hasan [24]	0.144	1.40	-
Pontaza [33]	0.140	1.48	0.141
Okajima [35] (Exp)	0.143	-	-

Table 5
Time convergence.

Time step (s)	2.4×10^{-2}	1.2×10^{-2}	6.0×10^{-3}	3.0×10^{-3}	Extrapolated value	Extrapolation order
Strouhal number	0.147239	0.147187	0.147170	0.147167	0.147166	1.79
Average drag coefficient	1.479280	1.478870	1.478765	1.478745	1.478739	2.04
r.m.s lift coefficient	0.143079	0.142748	0.142667	0.142652	0.142647	2.10

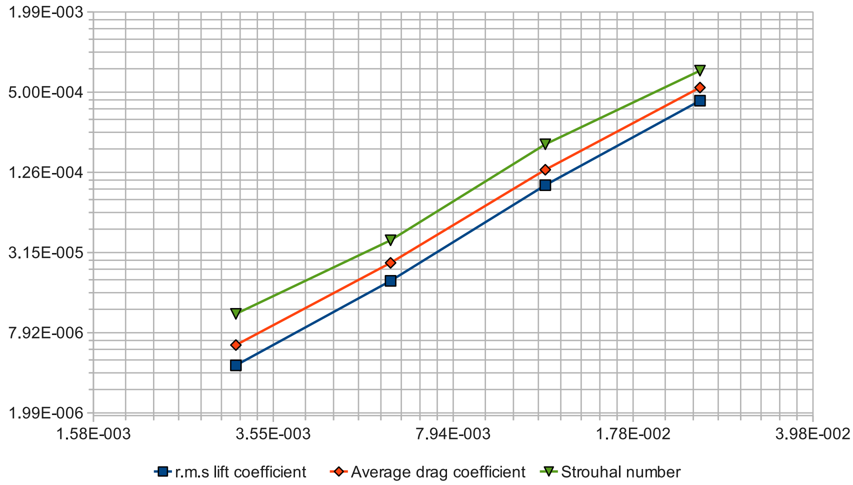

Fig. 13. Time convergence rates based on the extrapolation.

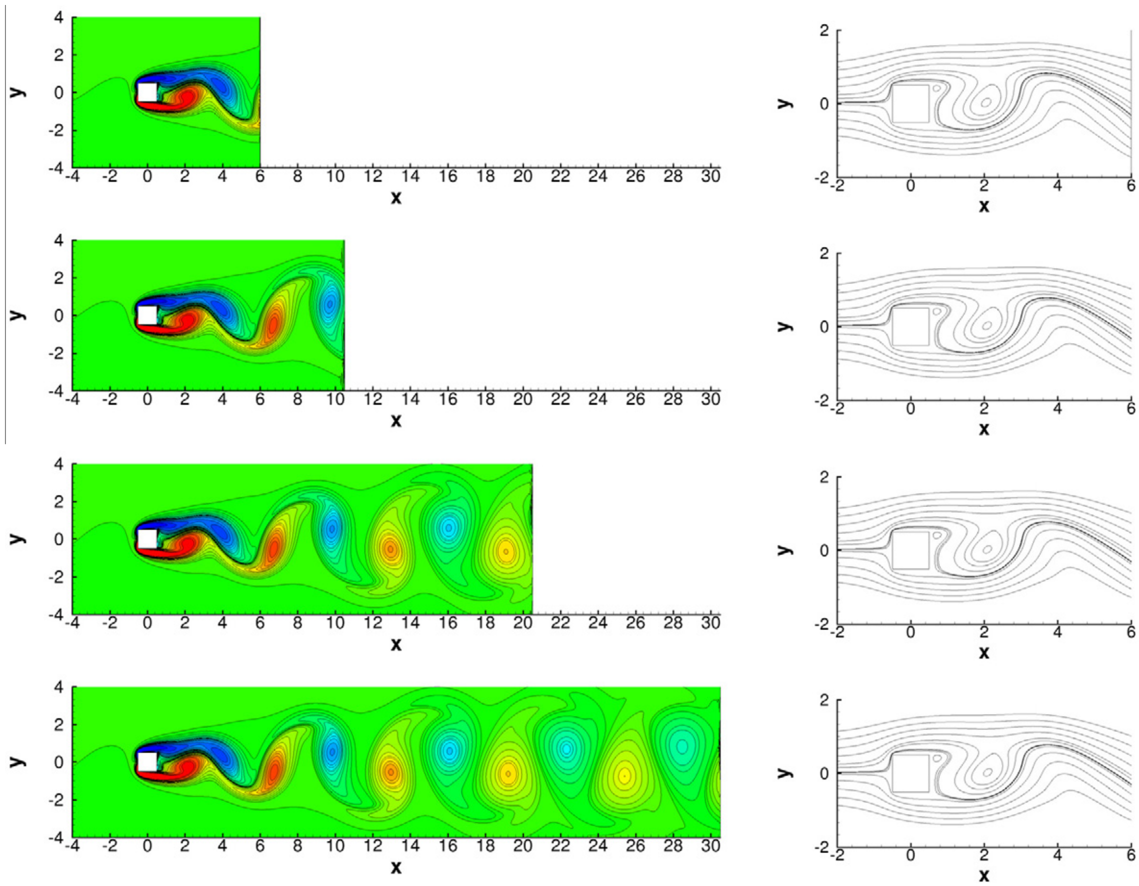

Fig. 14. Instantaneous vorticity contours (left) and streamlines (right) for four meshes, from top to bottom: Ω_1, Ω_2, Ω_3 and Ω_4. In order to compare, isovalues for vorticity contours are the same whatever the domain.

The values for five meshes are detailed in Table 1 and the convergence rates computed with the four finest meshes are in Table 2. A first order space convergence rate is obtained, which is caused, we presume, by the singularity of the geometry at the corners of the domain [40]. We verify on Fig. 11 that results are within the asymptotic convergence zone by plotting

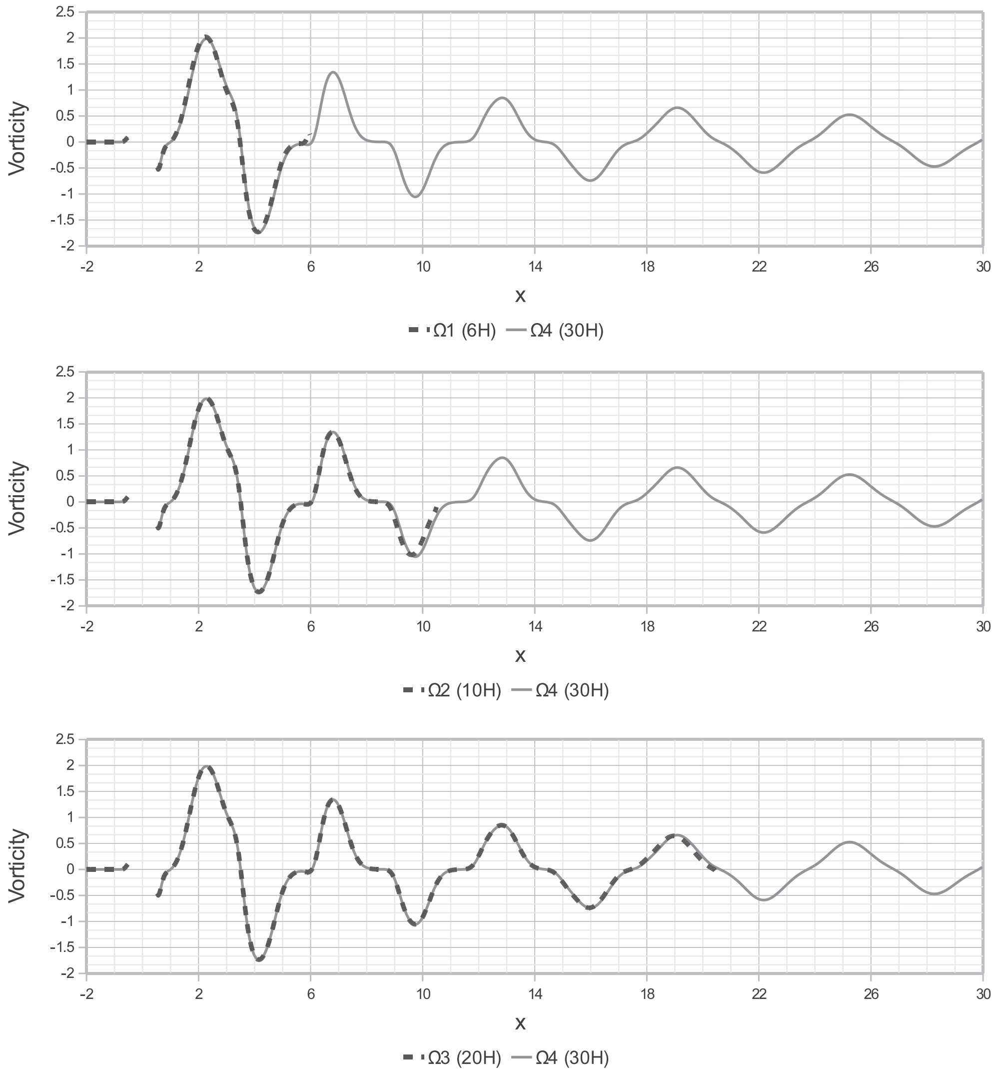

Fig. 15. Comparison of instantaneous vorticity along the line $y = 0$ between Ω_4 and the three other meshes.

the errors against the extrapolated solutions. Finally, we propose in Table 3 a detailed description of the eddies for five meshes: position (x_1,y_2) and vorticity (ω) at the center, and detachment and reattachment points coordinates.

5.3.2. Flow past a square section cylinder

We consider the two dimensional unsteady flow past a square cylinder studied by [34,36,24,33,35] with a normal incidence and $Re = 100$. The Reynolds number is based on the free-stream velocity ($u_\infty = 1\ \mathrm{m\,s^{-1}}$), the square width $H = 1$ m, the density $\rho = 1\ \mathrm{kg\,m^{-3}}$ and the viscosity $\nu = 0.001\ \mathrm{m^2\,s^{-1}}$. We consider four computational domains where the distance between the outflow boundary condition and the cylinder is, respectively, 6H, 10H, 20H and 30H:

- $\Omega_1 = [-10.5, 6.5] \times [-10.5, 10.5]$
- $\Omega_2 = [-10.5, 10.5] \times [-10.5, 10.5]$
- $\Omega_3 = [-10.5, 20.5] \times [-10.5, 10.5]$
- $\Omega_4 = [-10.5, 30.5] \times [-10.5, 10.5]$

The inflow boundary at $\{x_1 = -10.5\ \mathrm{m}\}$ is a Dirichlet condition set to a constant horizontal flow, the outflow boundary at $\{x_1 = 6.5\ \mathrm{m}\}$, $\{x_1 = 10.5\ \mathrm{m}\}$, $\{x_1 = 20.5\ \mathrm{m}\}$ or $\{x_1 = 30.5\ \mathrm{m}\}$ is the proposed open boundary condition OBC2. A symmetry condition is imposed on the upper and lower boundaries. No-slip condition is enforced on the square obstacle placed at $(x_1,x_2) = (0,0)$. The meshes have around two million points with a constant space step of 0.002 m in the sub-domain $[-2,4] \times [-2,2]$. Step size increases toward the boundaries. The initialisation of pressure is made with $p^0 = 0$. To destabilise the solution, an unsymmetrical velocity field is initialised: for $x_2 > 0$ $\boldsymbol{u}^0 = (1.1, 0)$ m and, for $x_2 < 0$, $\boldsymbol{u}^0 = (0.9, 0)$ m. The computations are made with $\Delta t = 0.003$ s.

The various global parameters characterising the flow are defined as:

- The lift coefficient $C_L = \frac{2F_{x_2}}{\rho u_\infty^2 H}$
- The drag coefficient $C_D = \frac{2F_{x_1}}{\rho u_\infty^2 H}$
- The Strouhal number $St = \frac{fH}{U_\infty}$

where f is the shedding frequency. F_{x_1} and F_{x_2} are the sums of both pressure and viscous forces in the x_1 and x_2 direction around the Γ_c boundary of the cylinder: $(F_{x_1}, F_{x_2}) = \int_{\Gamma_c} \sigma.\boldsymbol{n}$.

The result is a periodic Bénard-von Kármán vortex street shown on the Fig. 12. Values of the Strouhal number, the lift coefficient and the drag coefficient are detailed in Table 4, and are in agreement with the literature.

For the last domain Ω_4, we proceed to a time convergence study. Four time steps are chosen with a consecutive ratio of two. A convergence order around two is measured (see Table 5), in agreement with the formal convergence of the methods. We check on the Fig. 13 that the solutions are within the asymptotic convergence zone by plotting the errors against the extrapolated solutions.

Figs. 14 and 15 show the influence of the size of the computational domain on the rotational and the streamlines at the same phase (first time step just after sign change of the rotationnal at $(x, y) = (1, 0)$ m). As in [24], the position of the outflow boundary condition does not induce distortion of the vortices nor disturb flow around the cylinder. Nevertheless, we can see some distortions near the boundary condition, which reminds us that the open boundary condition is not a "universal" outlet boundary condition. These discrepancies are spatially limited to the boundary as shown on the Fig. 15 which represents vorticity profiles along the line $y = 0$.

References

[1] K.J. Arrow, L. Hurwicz, H. Uzawa, Studies in Linear and Non-Linear Programming, Stanford University Press, Stanford, 1958.
[2] M. Fortin, R. Glowinski, Méthodes de Lagrangien Augmenté – applications à la résolution numérique de problèmes aux limites, 1982.
[3] M.O. Deville, P.F. Fischer, E.H. Mund, High-Order Methods for Incompressible Fluid Flow, Cambridge University Press, Cambridge, 2002.
[4] V. Girault, P. Raviart, Finite Element Methods for Navier-Stokes Equations, Springer Verlag, Berlin, 1986.
[5] A. Chorin, Numerical solution of the Navier–Stokes equations, Mathematics of Computation 22 (1968) 745–762.
[6] R. Témam, Navier Stokes Equations: Theory and Numerical Analysis, North-Holland Pub. Co., Amsterdam, 1984.
[7] K. Goda, A multistep technique with implicit difference schemes for calculating two- or three-dimensional cavity flows, Journal of Computational Physics 30 (1979) 76–95.
[8] L.J.P. Timmermans, P.D. Minev, F.N. Van De Voss, An approximate projection scheme for incompressible flow using spectral elements, International Journal for Numerical Methods in Fluids 22 (1996) 673–688.
[9] J. Shen, On error estimates of the projection methods for the Navier–Stokes equations: Second-order schemes, Mathematics of Computation 65 (1996) 1039–1066.
[10] J.-L. Guermond, Calculation of incompressible viscous flows by an unconditionally stable projection FEM, Journal of Computational Physics 132 (1997) 12–33.
[11] J.-L. Guermond, P. Minev, J. Shen, An overview of projection methods for incompressible flows, Computer Methods in Applied Mechanics and Engineering 195 (2006) 6011–6045.
[12] S. Tsynkov, Numerical solution of problems on unbounded domains. A review, Applied Numerical Mathematics 27 (1998) 465–532.
[13] R.L. Sani, P.M. Gresho, Résumé and remarks on the open boundary condition minisymposium, International Journal for Numerical Methods in Fluids 18 (1994) 983–1008.
[14] I. Orlanski, A simple boundary condition for unbounded hyperbolic flows, Journal of Computational Physics 21 (1976) 251–269.
[15] B. Engquist, Absorbing boundary conditions for numerical simulation of waves, Proceedings of the National Academy of Sciences 74 (1977) 1765–1766.
[16] B. Engquist, A. Majda, Numerical radiation boundary conditions for unsteady transonic flow, Journal of Computational Physics 40 (1981) 91–103.
[17] G. Jin, M. Braza, A nonreflecting outlet boundary condition for incompressible unsteady Navier–Stokes calculations, Journal of Computational Physics 107 (1993) 239–253.
[18] M. Forestier, R. Pasquetti, R. Peyret, Spatial development of wakes using a spectral multi-domain method, Applied Numerical 33 (2000) 207–216. C.
[19] M.V. Salvetti, P. Orlandi, R. Verzicco, Numerical simulations of transitional axisymmetric coaxial jets, AIAA Journal 34 (1996) 736–743.
[20] J. Liu, Open and traction boundary conditions for the incompressible NavierStokes equations, Journal of Computational Physics 228 (2009) 7250–7267.
[21] D. Coutand, S. Shkoller, On the interaction between quasilinear elastodynamics and the Navier–Stokes equations, Archive for Rational Mechanics and Analysis 179 (2005) 303–352.
[22] J.-L. Guermond, P. Minev, J. Shen, Error analysis of pressure-correction schemes for the time-dependent stokes equations with open boundary conditions, SIAM Journal on Numerical Analysis 43 (2005) 239–258.
[23] C.-H. Bruneau, P. Fabrie, Effective downstream boundary conditions for incompressible Navier–Stokes equations, International Journal for Numerical Methods in Fluids 19 (1994) 693–705.
[24] N. Hasan, S. Anwer, S. Sanghi, On the outflow boundary condition for external incompressible flows: a new approach, Journal of Computational Physics 206 (2005) 661–683.
[25] C. Févrière, J. Laminie, P. Poullet, P. Angot, On the penalty-projection method for the NavierStokes equations with the MAC mesh, Journal of Computational and Applied Mathematics 226 (2009) 228–245.
[26] M. Kirkpatrick, S. Armfield, Open boundary conditions in numerical simulations of unsteady incompressible flow, ANZIAM Journal 50 (2008) 760–773.
[27] F.H. Harlow, J.E. Welch, Numerical calculation of time-dependent viscous incompressible flow of fluid with free surface, Physics of Fluids 8 (1965) 2182–2189.
[28] E. Ahusborde, S. Glockner, A 2D block-structured mesh partitioner for accurate flow simulations on non-rectangular geometries, Computers & Fluids 43 (2011) 2–13.
[29] Hypre, Hypre high performance preconditionner user's manual, <http://acts.nersc.gov/hypre/>, Center for Applied Scientific Computing, Lawrence Livermore National Laboratory, 2008.

[30] P. Amestoy, Multifrontal parallel distributed symmetric and unsymmetric solvers, Computer Methods in Applied Mechanics and Engineering 184 (2000) 501–520.
[31] S. Schaffer, A semicoarsening multigrid method for elliptic partial differential equations with highly discontinuous and anisotropic coefficients, SIAM Journal on Scientific Computing 20 (1998) 228–242.
[32] P.N. Brown, R.D. Falgout, J.E. Jones, Semicoarsening multigrid on distributed memory machines, SIAM Journal on Scientific Computing 21 (2000) 1823.
[33] J. Pontaza, J. Reddy, Least-squares finite element formulations for viscous incompressible and compressible fluid flows, Computer Methods in Applied Mechanics and Engineering 195 (2006) 2454–2494.
[34] A. Sohankar, C. Norberg, L. Davidson, Low-Reynolds-number flow around a square cylinder at incidence: study of blockage, onset of vortex shedding and outlet boundary condition, International Journal for Numerical Methods in Fluids 26 (1998) 39–56.
[35] A. Okajima, Strouhal numbers of rectangular cylinders, Journal of Fluid Mechanics 123 (2006) 379–398.
[36] A. Pavlov, S. Sazhin, R. Fedorenko, A conservative finite difference method and its application for the analysis of a transient flow around a square prism, Methods for Heat and Fluid Flow 10 (2000) 6–46.
[37] H.K. Moffatt, Viscous and resistive eddies near a sharp corner, Journal of Fluid Mechanics 18 (2006) 1–18.
[38] J. Richardson, L.F. Gaunt, The deferred approach to the limit. Part I. Single lattice. Part II. Interpenetrating lattices, Philosophical Transactions of the Royal Society of London. Series A, Containing Papers of a Mathematical or Physical Character 226 (1927) 299–361.
[39] P.J. Roache, Verification and Validation in Computational Science and Engineering, Hermosa Publishers, Albuquerque, 1998.
[40] M. Dauge, Elliptic boundary value problems in corner domains, Lecture Notes in Mathematics 1341 (1988) 1–257.